

Lessons from the Auriga discs: The hunt for the Milky Way’s ex-situ disc is not yet over

Facundo A. Gómez^{1*}, Robert J. J. Grand^{2,3}, Antonela Monachesi¹,
Simon D. M. White¹, Sebastian Bustamante², Federico Marinacci⁴,
Rüdiger Pakmor², Christine M. Simpson², Volker Springel^{2,3}, and Carlos S. Frenk⁵

¹*Max-Planck-Institut für Astrophysik, Karl-Schwarzschild-Str. 1, D-85748, Garching, Germany*

²*Heidelberger Institut für Theoretische Studien, Schloss-Wolfsbrunnengasse 35, 69118 Heidelberg, Germany*

³*Zentrum für Astronomie der Universität Heidelberg, Astronomisches Recheninstitut, Monchhofstr. 12-14, 69120 Heidelberg, Germany*

⁴*Department of Physics, Kavli Institute for Astrophysics and Space Research, MIT, Cambridge, MA 02139, USA*

⁵*Institute for Computational Cosmology, Department of Physics, Durham University, South Road, Durham, DH1 3LE, UK*

ABSTRACT

We characterize the contribution from accreted material to the galactic discs of the Auriga Project, a set of high resolution magnetohydrodynamic cosmological simulations of late-type galaxies performed with the moving-mesh code AREPO. Our goal is to explore whether a significant accreted (or ex-situ) stellar component in the Milky Way disc could be hidden within the near-circular orbit population, which is strongly dominated by stars born in-situ. One third of our models shows a significant ex-situ disc but this fraction would be larger if constraints on orbital circularity were relaxed. Most of the ex-situ material ($\gtrsim 50\%$) comes from single massive satellites ($> 6 \times 10^{10} M_{\odot}$). These satellites are accreted with a wide range of infall times and inclination angles (up to 85°). Ex-situ discs are thicker, older and more metal-poor than their in-situ counterparts. They show a flat median age profile, which differs from the negative gradient observed in the in-situ component. As a result, the likelihood of identifying an ex-situ disc in samples of old stars on near-circular orbits increases towards the outskirts of the disc. We show three examples that, in addition to ex-situ discs, have a strongly rotating dark matter component. Interestingly, two of these ex-situ stellar discs show an orbital circularity distribution that is consistent with that of the in-situ disc. Thus, they would not be detected in typical kinematic studies.

Key words: Galaxy: disc – Galaxy: evolution – galaxies: evolution – galaxies: interactions – galaxies: kinematics and dynamics – methods: numerical.

1 INTRODUCTION

According to the currently favored cosmological model, Λ cold dark matter (Λ CDM), galaxies like our own merge and interact with companions of widely different masses throughout their history (Springel et al. 2008). The quantification and characterization of the merger activity that a galaxy has undergone can thus be used to constrain galaxy formation models.

Mergers and interactions with very low mass satellites (masses $\lesssim 10^7 M_{\odot}$) are difficult to detect since such satellites are expected to possess, if any, only a small number of stars (see Sawala et al. 2016, and references therein). The detection of truly “dark” satellites would be extremely rewarding

as it could put stringent constraints on the nature of DM (e.g. Springel et al. 2008; Vogelsberger et al. 2012; Macciò et al. 2013; Li et al. 2016; Bose et al. 2017). Nonetheless, an undisputed detection of this type of substructure is yet to be made.

The identification of mergers associated with intermediate mass satellites (i.e. masses $< 10\%$ of the host mass) is significantly less challenging. As such satellites interact with the host gravitational potential, they are tidally disrupted leaving behind debris in the form of stellar streams. Depending on the time since disruption this debris can be detected either in real space, in the form of extended cold streams (recent disruption) (e.g. Ibata et al. 1994, 2001; Belokurov et al. 2006, 2007), or as clumps in the space of quasi-conserved integrals of motions (well after disruption) (Helmi et al. 1999, 2006; Klement et al. 2009; Morrison et al. 2009; Helmi et al.

* E-mail: fgomez@mpa-garching.mpg.de

2014). In the Milky Way several streams have been identified and, in some cases, their progenitors have been characterized. However, a robust quantification of our Galaxy's merger activity is still lacking. The main reason for this has been the lack of sufficiently large and accurate full phase-space catalogs that could unveil debris from early accretion events, which would be generally be deposited in the inner Galactic regions. Thanks to the astrometric satellite *Gaia* (Gaia Collaboration et al. 2016), in combination with previous and upcoming spectroscopic surveys (e.g. Steinmetz et al. 2006; Gilmore et al. 2012; Cui et al. 2012; de Jong et al. 2014; Dalton 2016), this will soon be possible (Helmi & de Zeeuw 2000; Gómez et al. 2010). Indeed, the first *Gaia* data release has started to uncover previously unknown substructure in the Galactic stellar halo (Helmi et al. 2017).

Isolating debris from more massive merger (i.e. masses $\geq 10\%$ of the host mass) is, however, more challenging. As discussed by Ruchti et al. (2014, hereafter R14), the reason for this is two-fold. First, dynamical friction is most efficient for these massive objects. They are quickly dragged to small radii where the mixing time scales are short. Second, debris from these satellites is kinematically hotter than that from smaller mass objects and thus mixes faster. Relatively massive mergers can be detected indirectly, by searching for perturbations in the local velocity field of the Galactic disc, both in-plane (Minchev et al. 2009; Gómez et al. 2012) and perpendicular to the Galactic plane (Gómez et al. 2013; Widrow et al. 2014). Substructure in the local disc velocity field has already been identified (Minchev et al. 2009; Gómez et al. 2012; Widrow et al. 2012). However, perturbations from the Galactic bar or spiral arms and debris from significantly less massive satellites may explain much of this substructure (e.g. Helmi et al. 2006; Arifanto & Fuchs 2006; Klement et al. 2008; Antoja et al. 2009; Monari et al. 2016).

The addition of extra dimensions to the analysis, based on chemical abundances patterns and stellar ages, is thus crucial to isolate debris coming from individual progenitors (Helmi et al. 2014; Minchev et al. 2014b; Ruchti et al. 2014, 2015). Indeed, Ruchti et al. (2015, hereafter R15) analyzed a sample of ~ 5000 stars from the *Gaia*-ESO survey with full phase-space, [Mg/Fe] and [Fe/H] measurements to search for signatures of the most massive merger events our Galaxy has undergone. Their efforts were focused on the identification of an accreted or ex-situ disc component. Such an ex-situ disc is expected to arise during massive mergers at low inclination angles with respect to the plane of the main disc (Abadi et al. 2003; Read et al. 2008, 2009; Purcell et al. 2009; Pillepich et al. 2014, 2015; Schaller et al. 2016). A DM disc may also form at the same time, which could have important consequences for direct DM detection experiments (see Schaller et al. 2016, and references therein). To select ex-situ disc star candidates, R15 used a chemodynamical template first introduced by R14. As they discussed, for $[\text{Fe}/\text{H}] > -1.3$, stellar populations of surviving dwarf galaxies generally have $[\text{Mg}/\text{Fe}] < 0.3$, which is lower than typical MW stars at the same $[\text{Fe}/\text{H}]$. To further isolate ex-situ disc candidates, R14 focused on stars co-rotating with the disc on orbits with significant eccentricity. Debris from massive mergers is expected to lie preferentially on such orbits. Both R14 and R15 found no evidence of a significant prograde ex-situ disc component of this type. They concluded that the

MW has no significant ex-situ stellar disc, and thus possesses no significant DM disc formed by a merger.

In this paper we study the formation of ex-situ stellar discs in the Auriga simulations, a set of high-resolution magneto-hydrodynamic simulations of disc galaxy formation from Λ CDM initial conditions (Grand et al. 2017). *Our goal is to explore whether a significant ex-situ stellar disc component could be hidden within the near-circular orbit population, which is strongly dominated by in-situ stars.* In Section 2 we introduce the Auriga suite. We define our ex-situ discs in Section 3 and quantify the number of models with a significant such component in Section 4. In Section 5 we show how our ex-situ discs are formed, and we characterize their main stellar populations properties in Section 6. In Section 7 we discuss how these discs might be detected with upcoming observational campaigns. We discuss the implications of our findings for a possible ex-situ stellar and DM discs in our Galaxy in Section 8. We conclude in Section 9.

2 THE AURIGA SIMULATIONS

In this paper we analyze a subsample of the cosmological magnetohydrodynamic simulations of the Auriga suite (Grand et al. 2017, hereafter GR17). In what follows we summarize the main characteristics of these simulations. For a more detailed description we refer the reader to GR17.

The Auriga suite is composed of 30 high-resolution cosmological zoom-in simulations of the formation of late-type galaxies within Milky Way-sized haloes. The haloes were selected from a lower resolution dark matter only simulation from the Eagle Project (Schaye et al. 2015), a periodic box of side 100 Mpc. Each halo was chosen to have, at $z = 0$, a virial mass in the range of $10^{12} - 2 \times 10^{12} M_{\odot}$ and to be more distant than nine times the virial radius from any other halo of mass more than 3% of its own mass. Each halo was run at multiple resolution levels. The typical dark matter particle and gas cell mass resolutions for the simulations used in this work (Auriga level 4) are $\sim 3 \times 10^5 M_{\odot}$ and $\sim 5 \times 10^4 M_{\odot}$, respectively. The gravitational softening length used for stars and DM grows with scale factor up to a maximum of 369 pc, after which it is kept constant in physical units. The softening length of gas cells scales with the mean radius of the cell, but is never allowed to drop below the stellar softening length. A resolution study across three resolution levels (GR17) shows that many galaxy properties, such as surface density profiles, orbital circularity distributions, star formation histories and disc vertical structures are already well converged at the resolution level used in this work.

The simulations were carried out using the N -body + moving-mesh, magnetohydrodynamics code AREPO (Springel 2010; Pakmor et al. 2016). A Λ CDM cosmology, with parameters $\Omega_m = \Omega_{\text{dm}} + \Omega_b = 0.307$, $\Omega_b = 0.048$, $\Omega_{\Lambda} = 0.693$, and Hubble constant $H_0 = 100 h \text{ km s}^{-1} \text{ Mpc}^{-1} = 67.77 \text{ km s}^{-1} \text{ Mpc}^{-1}$, was adopted.

The baryonic physics model used in these simulations is a slightly updated version of that in Marinacci et al. (2014). It follows a number of processes that play a key role in the formation of late-type galaxies, such as gas cooling/heating, star formation, mass return and metal enrichment from stellar evolution, the growth of supermassive black holes, and feedback both from stellar sources and from black hole ac-

Table 1. Table of simulation parameters. The columns are 1) Model name; 2) Virial mass; 3) Virial radius; 4) Stellar mass; 5) Disc stellar mass; 6) Disc radial scale length; 7) Bulge stellar mass; 8) Bulge effective radius; 9) Sersic index of the bulge, 10) Disc to total mass ratio and 11) Optical radius. See GR17 for definitions.

Run	M_{vir} [$10^{10} M_{\odot}$]	R_{vir} [kpc]	M_{\star} [$10^{10} M_{\odot}$]	M_{d} [$10^{10} M_{\odot}$]	R_{d} [kpc]	M_{b} [$10^{10} M_{\odot}$]	R_{eff} [kpc]	n	D/T	R_{opt} [kpc]
Au-2	191.466	261.757	7.045	6.377	11.644	2.341	2.056	1.529	0.73	37.0
Au-3	145.777	239.019	7.745	6.288	7.258	2.039	1.488	0.987	0.76	31.0
Au-4	140.885	236.310	7.095	3.662	3.929	2.005	1.740	1.352	0.65	24.5
Au-5	118.553	223.091	6.722	4.509	3.583	1.806	0.839	0.874	0.71	21.0
Au-6	104.385	213.825	4.752	3.315	5.949	1.649	2.851	2.000	0.67	26.0
Au-7	112.043	218.935	4.875	2.458	5.140	2.045	1.731	1.740	0.55	25.0
Au-8	108.062	216.314	2.990	2.457	6.572	0.652	2.147	1.328	0.79	25.0
Au-9	104.971	214.224	6.103	3.597	3.367	2.169	0.999	0.948	0.62	19.0
Au-10	104.710	214.061	5.939	2.378	2.596	3.152	1.080	1.181	0.43	16.0
Au-12	109.275	217.117	6.010	4.315	3.290	1.134	0.892	0.759	0.79	19.0
Au-13	118.904	223.325	6.194	1.675	3.382	3.798	1.403	1.549	0.31	15.5
Au-14	165.721	249.442	10.393	6.359	4.186	3.184	1.138	1.586	0.67	26.0
Au-15	122.247	225.400	3.930	2.772	5.320	1.047	2.216	2.000	0.73	23.0
Au-16	150.332	241.480	5.410	5.059	9.030	1.175	1.825	1.391	0.81	36.0
Au-17	102.835	212.769	7.608	2.563	4.191	4.641	1.208	0.831	0.36	16.0
Au-18	122.074	225.288	8.037	5.205	3.719	2.461	1.225	0.950	0.68	21.0
Au-19	120.897	224.568	5.320	3.532	4.805	1.428	1.416	2.000	0.71	24.0
Au-20	124.922	227.028	4.740	2.248	8.019	2.353	2.174	1.886	0.49	30.0
Au-21	145.090	238.645	7.717	6.005	4.607	1.240	1.188	1.064	0.83	24.0
Au-22	92.621	205.476	6.020	2.851	2.249	2.709	1.014	0.934	0.51	13.5
Au-23	157.539	245.274	9.023	5.547	4.985	3.192	1.708	1.438	0.63	25.0
Au-24	149.178	240.856	6.554	3.756	5.570	2.186	0.946	0.969	0.63	30.0
Au-25	122.109	225.305	3.142	2.475	6.695	0.934	2.951	1.879	0.73	21.0
Au-26	156.384	244.685	10.967	4.697	3.141	5.456	1.116	1.017	0.46	18.0
Au-27	174.545	253.806	9.606	7.229	4.287	1.742	0.947	1.065	0.81	26.0
Au-28	160.538	246.833	10.448	6.761	2.159	2.359	0.948	1.109	0.74	17.5

cretion. In addition, magnetic fields were implemented as described in Pakmor & Springel (2013). The effect of these magnetic fields on the global evolution of the Auriga galaxies is discussed in detail in Pakmor et al. (2017). The parameters that regulate the efficiency of each physical process were chosen by comparing the results obtained in simulations of cosmologically representative regions to a wide range of observations of the galaxy population (Vogelsberger et al. 2013; Marinacci et al. 2014).

From now on, we will refer to these simulations as Au- i , with i enumerating the different initial conditions. We will focus on the subset of 26 models that, at the present-day, show a well defined stellar disc. The main properties of each simulated galaxy are listed in Table 1. The disc/bulge decomposition is made by simultaneously fitting exponential and Sersic profiles to the stellar surface face-on density profiles. A detailed description of how these parameters were obtained is given in GR17.

3 EX-SITU DISC DEFINITION

The goal of this work is to characterize the contribution from ex-situ formed (accreted)¹ material to the Auriga stellar discs. In what follows we will designate as ex-situ all star particles formed within the potential well of a self-bound

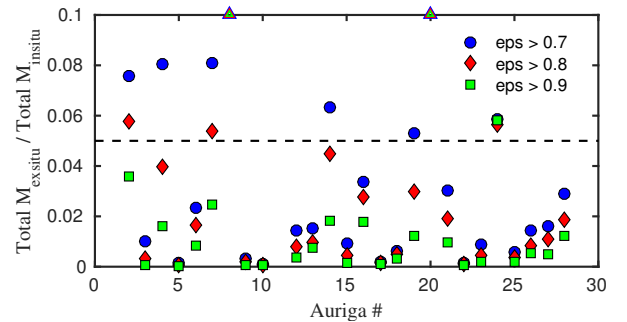


Figure 1. Ratio of the total ex-situ to in-situ disc mass, η , for the different Auriga galaxies. Only stellar particles with $R < R_{\text{opt}}$ and $|Z| < 10$ kpc are considered. Blue, red and green symbols indicate the results obtained when a cut in the circularity parameter at 0.7, 0.8 and 0.9 is imposed, respectively. The horizontal dashed lines indicate a 5% mass ratio.

satellite galaxy prior to its disruption. At the present-day, such star particles can either belong to the main host, after being tidally stripped from their progenitor, or they can still be bound to this progenitor. Conversely, following Cooper et al. (2015), all particles formed within the potential well of the main host halo will be referred to as in-situ star particles. Note that, contrary to Pillepich et al. (2015), this definition includes star particles formed within the host virial radius out of gas recently stripped from satellites. These stellar particles are not found in the galactic disc and thus do not affect our results.

¹ In this work the terms ex-situ and accreted are used interchangeably.

To define star particles that are in the galactic disc we perform a kinematic decomposition based on the circularity parameter, ϵ . Following [Abadi et al. \(2003\)](#), this parameter is defined as

$$\epsilon = \frac{L_z}{L_z^{\max}(E)}, \quad (1)$$

where L_z is the Z -component of angular momentum of a given star particle and $L_z^{\max}(E)$ is the maximum angular momentum allowed for its orbital energy, E . Before computing the star particle's angular momentum, each galaxy is re-oriented as described in GR17, i.e., the Z -axis direction is defined through the semi-minor axis of the moment of inertia tensor of the star particles within $0.1R_{200}$.

All star particles that satisfy *i*) $\epsilon \geq 0.7$, *ii*) $|Z| < 10$ kpc and *iii*) $R < R_{\text{opt}}$ are considered as disc star particles, independently of birth location. Here R is the galactocentric cylindrical distance and R_{opt} is the galactic optical radius, defined as the 25 mag arcsec⁻² B-band isophotal radius ([Binney & Merrifield 1998](#)). To minimize contamination from stellar halo populations, for significantly lopsided galaxies R_{opt} is defined as the minimum cylindrical radius where $\mu_B = 25$ mag arcsec⁻².

4 EX-SITU DISC QUANTIFICATION

In this Section we quantify the number of Auriga galaxies that possesses a significant ex-situ disc. To identify such discs we show in Figure 1 the ratio of total ex-situ to in-situ disc mass, $\eta = M_{\text{exsitu}}^{\text{tot}}/M_{\text{insitu}}^{\text{tot}}$, for all our galactic discs. Interestingly, 31% (8) of our disc sample show a significant ex-situ disc, defined as $\eta \gtrsim 0.05$ (dashed line). The two largest ex-situ discs, Au-8 and Au-20 have η of ~ 0.15 and ~ 0.3 , respectively. In general, the value of η rapidly decreases as we increase the circularity threshold from $\epsilon = 0.7$ to 0.9. This is not surprising since the orbital eccentricity of ex-situ disc stars is expected to be, on average, larger than that of their in-situ counterparts (see e.g. [Sales et al. 2009](#)).

Figure 2 shows the surface density ratio, $\mu = \Sigma_{\text{exsitu}}/\Sigma_{\text{insitu}}$, as a function of galactocentric distance. To allow a direct comparison, distances are normalized by the corresponding R_{opt} . Note that, in general, μ has a rising profile. This indicates that the relative contribution of ex-situ material to the disc rises as we move towards the outer disc regions. In the most extreme case, Au-14, μ varies by approximately two orders of magnitudes within R_{opt} .

Two-thirds of our disc sample shows either a very small or a negligible fraction of ex-situ material. Thus, in what follows, we will focus on the subsample of galaxies with significant ex-situ discs ($\eta > 0.05$).

Figure 3 shows the B-band surface brightness maps of these galaxies, obtained considering only ex-situ star particles. In this figure we include all ex-situ star particles that at the present-day belong to the main host, independently of their circularity parameter. Thus, stellar populations that belong to the galactic spheroid, or stellar halo, are also included. In general, the ex-situ material shows a mildly oblate distribution, flattened along the Z -direction (e.g. [McCarthy et al. 2012](#); [Monachesi et al. 2016](#), [Monachesi et al. 2017](#)). Only galaxies Au-2, Au-8, and Au-24 show a significantly

flattened distribution that visually resembles the structure expected for a stellar disc. In some cases, such as Au-14, Au-19 and Au-20, clear signatures of cold substructure can be observed. This is debris from recent or on-going disruption events, which crosses the inner galactic regions, but has not yet had time to fully mix.

Figure 4 shows B-band surface brightness maps of the same galaxies, now obtained using only ex-situ star particles that satisfy the condition $\epsilon \geq 0.7$. This figure exposes, in all cases, a clear ex-situ disc component composed of star particles on near-circular orbits. As discussed before, some of these ex-situ discs (e.g. Au-14 and Au-19), show several spatially coherent stellar streams, associated with recent accretion events. On the other hand, discs such as Au-2 show a very smooth spatial distribution. As we show below, the Au-2 ex-situ disc formed as a result of two $\sim 1 : 10$ mergers that took place 8 Gyr ago, giving enough time for the resulting debris to fully mix.

In Figure 5 we show the circularity (ϵ) distribution of all star particles (black lines) that are located within our spatial disc selection box, i.e. $R < R_{\text{opt}}$ and $|Z| < 10$ kpc, obtained from galaxies with significant ex-situ disc components. The blue and red lines show the contribution from the in-situ and ex-situ stellar populations, respectively. Interestingly, in half of our sample, the circularity distribution of the ex-situ component peaks at values of $\epsilon < 0.7$ (Au-4, Au-7, Au-19 and Au-20). However, for the remaining half, it peaks at $\epsilon \geq 0.7$. Note that, as discussed in Section 1, previous studies that attempted to identify an ex-situ component in the Milky Way disc have focused their analysis on stellar samples with $0.2 < \epsilon < 0.8$ (R14, R15). This selection criterion is clearly justified by the complexity of detecting an ex-situ component on in-situ dominated near-circular orbits ($\epsilon > 0.7$). However, this figure shows that most stars of a hypothetical accreted Milky Way disc could be buried in this region.

5 FORMATION OF EX-SITU DISCS

In this section we explore how and when these ex-situ discs are formed. In particular, we are interested in characterizing the number, orbital properties, and the total and stellar mass spectrum of the satellites that have contributed to their formation.

In Figure 6 we decompose the total ex-situ disc mass into different accreted satellite contributors. Satellites are ranked according to their fractional mass contribution in decreasing order (i.e. the larger the contributor, the smaller the rank assigned). Interestingly, we find that only a few satellites are needed to account for the bulk of the mass of the ex-situ discs. The number of significant contributors, defined as the number of satellites required to account for 90% of the mass, ranges from 1 to 3, with a median of 2. This is smaller than the number of significant contributors that build up the accreted stellar halos of these galaxies, which ranges between 3 to 8, with a median of 5 ([Cooper et al. 2010](#), [Monachesi et al. 2017](#)). Note as well that, in all cases, there is a dominant contributor that accounts for $\gtrsim 50\%$ of the total mass.

In Table 2 we list some of the main properties of the most significant contributor to each ex-situ disc. Second con-

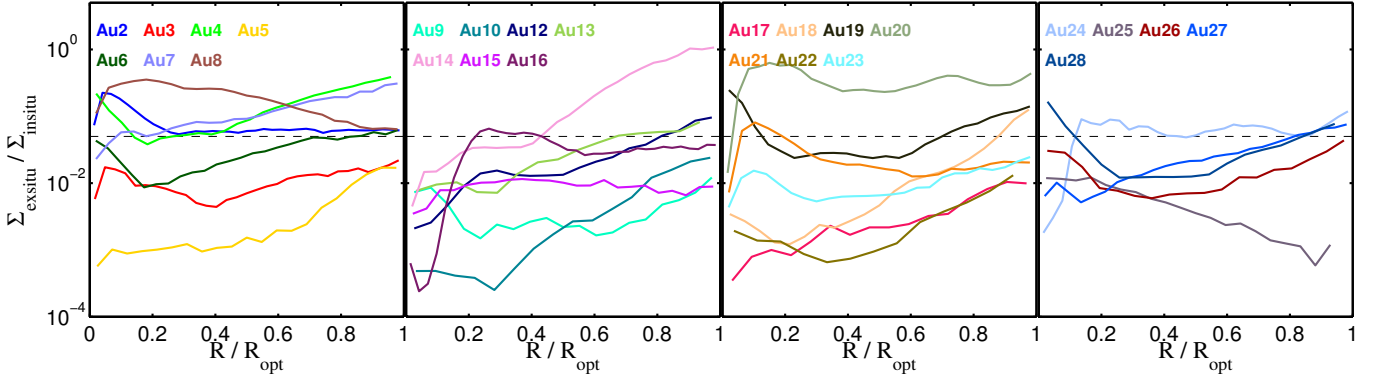


Figure 2. Surface density ratio, $\mu = \Sigma_{\text{exsitu}}/\Sigma_{\text{insitu}}$, as a function of galactocentric distance for the different Auriga galaxies. For comparison, distances are normalized by the corresponding R_{opt} . The horizontal dashed lines indicate a 5% density ratio.

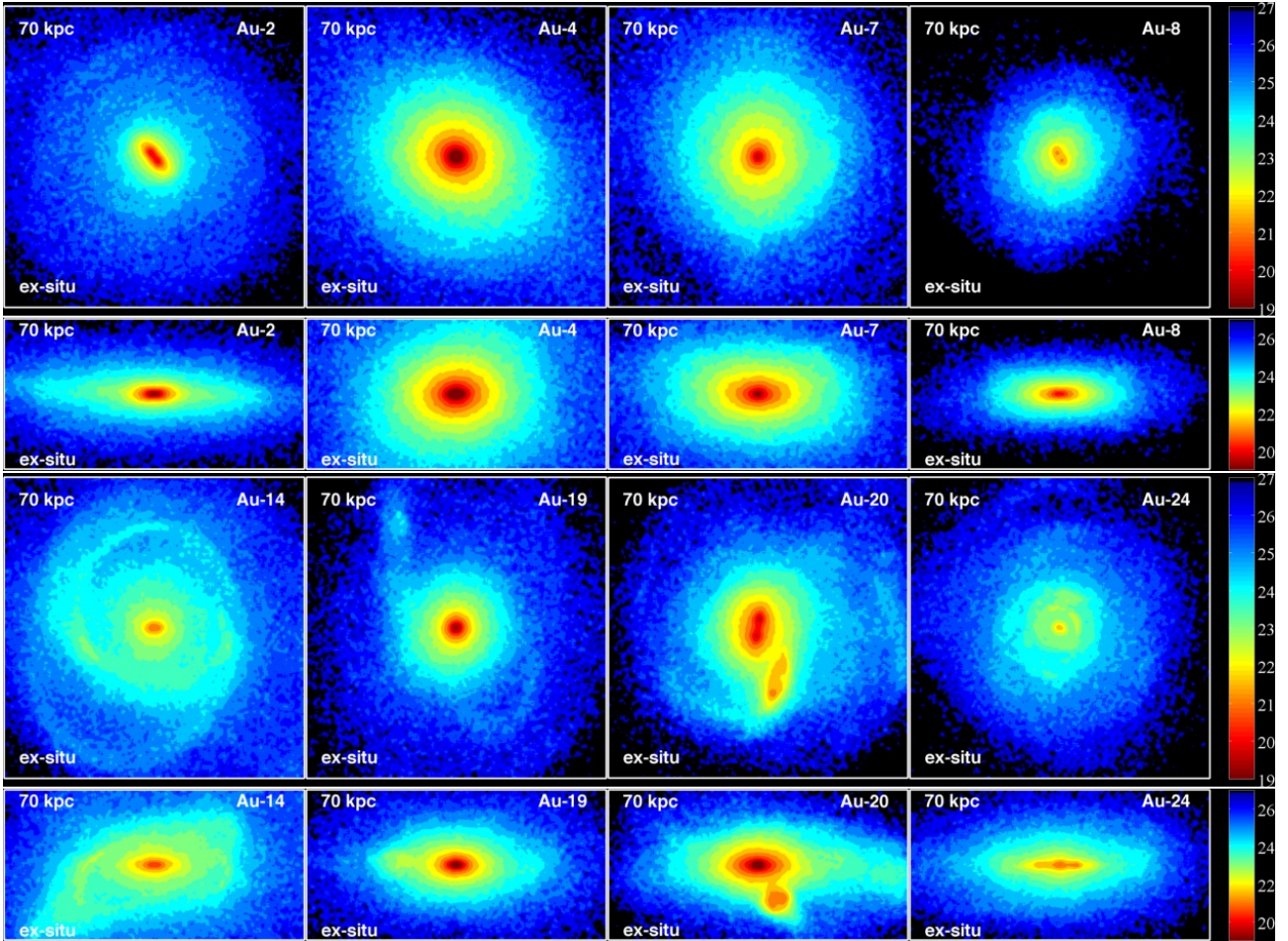


Figure 3. Present-day face-on and edge-on images of the B-band surface brightness of galaxies that show a significant ex-situ disc. In this figure all ex-situ star particles are considered, independent of their circularity parameter. Only particles that belong to the main host are considered. The side length of each panel is 70 kpc. The colour bar indicates the scale for μ_B in units of mag arcsec^{-2} .

tributors are listed in those cases where their contribution is also significant ($\gtrsim 20\%$ of the ex-situ disc mass). In several cases, we find that the most significant contributors are massive satellites. Their peak total masses, i.e. the maximum instantaneous mass that these satellites have reached,

are $M_{\text{sat}}^{\text{peak}} > 10^{11} M_{\odot}$. Thus, they are associated with large merger events. However, we also find cases in which these satellites have relatively low mass. The peak masses of the significant contributors range from $0.6 \times 10^{11} M_{\odot}$ (Au-24) to $5.3 \times 10^{11} M_{\odot}$ (Au-4). As expected, second significant

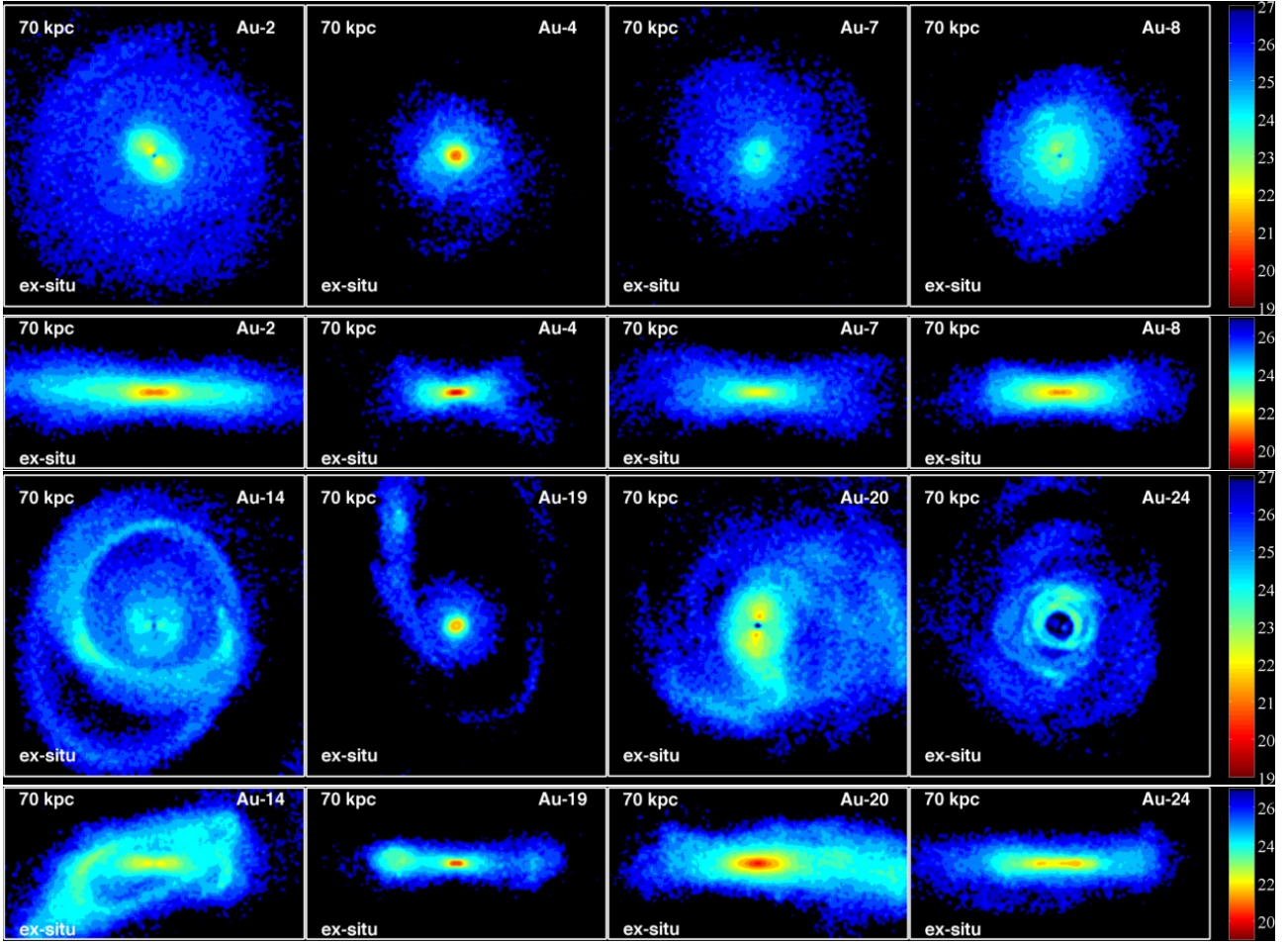


Figure 4. As in Figure 3 but for ex-situ star particles with circularity parameter $\epsilon \geq 0.7$. Note that, even though the side length of each panel is in all cases 70 kpc, only star particles located within $R < R_{\text{opt}}$ and $|Z| < 10$ kpc are considered as members of the ex-situ discs.

contributors are associated with less massive satellites. We note that, in all these cases, M_{peak} is achieved just prior to infall through the host virial radius.

Table 2 also lists the lookback time, t_{cross} , at which each satellite first crosses the host virial radius, R_{vir} , for the first time. The dispersion in t_{cross} values is large, ranging from early infall events with $t_{\text{cross}} = 9.1$ Gyr (Au-14) to very late infall events with $t_{\text{cross}} = 3.1$ Gyr (Au-4). Au-4 is an interesting case in which the host undergoes a major merger of mass ratio $M_{\text{sat}}/M_{\text{host}} \approx 0.67$, approximately 3 Gyr ago. The host disc is strongly perturbed but survives the interaction and quickly regrows (within 2 Gyr) to reach a present-day optical radius of $R_{\text{opt}} = 24.5$ kpc.

Finally, Table 2 lists the satellite’s infalling angle, θ_{infall} , defined as the angle between the disc angular momentum and that of the satellite’s orbit, both measured at t_{cross} . Again we find a large spread in θ_{infall} , with values that range from 15° (Au-20) to 85° (Au-7). Significant ex-situ discs are expected to form from mergers events in which massive satellites are accreted with low grazing angles, such as Au-20. Ex-situ discs formed as a result of mergers with massive satellites that are accreted with large θ_{infall} are more interesting and thus we study them in more detail.

In the top panels of Figure 7 we show with red (blue)

lines the time evolution of the angle between the disc angular momentum and the most significant (second) contributor orbital angular momentum vectors. Only four representative examples are shown, but similar results are found for the remaining galaxies. It is interesting to notice how these massive satellites start to align with the host disc as soon as, or even before, they cross the host R_{vir} . This is particularly clear in Au-2. The angle between the disc and the two most significant contributors before they cross R_{vir} , ~ 9 Gyr ago, is $\sim 60^\circ$ and 70° , respectively. For reference, we show in the bottom panels of Fig. 7 the time evolution of the satellites’ galactocentric distances, R_{s1} and R_{s2} , and of the host virial radius, R_{vir} . In many cases, it only takes ~ 2 Gyr for these satellites to become almost perfectly aligned with the host disc.

A very similar situation can be seen in the remaining examples. Note that the rapid alignment between these two angular momentum vectors is due not only to changes in the orbits of the satellite galaxies, but also to a strong response of the host galactic discs. This can be seen in the top panels of Fig. 7 where we show, with black lines, the time evolution of the disc’s angular momentum vector orientation with respect to its orientation at the present-day. In general, the discs start to rapidly tilt as soon as the satellites cross R_{vir} ,

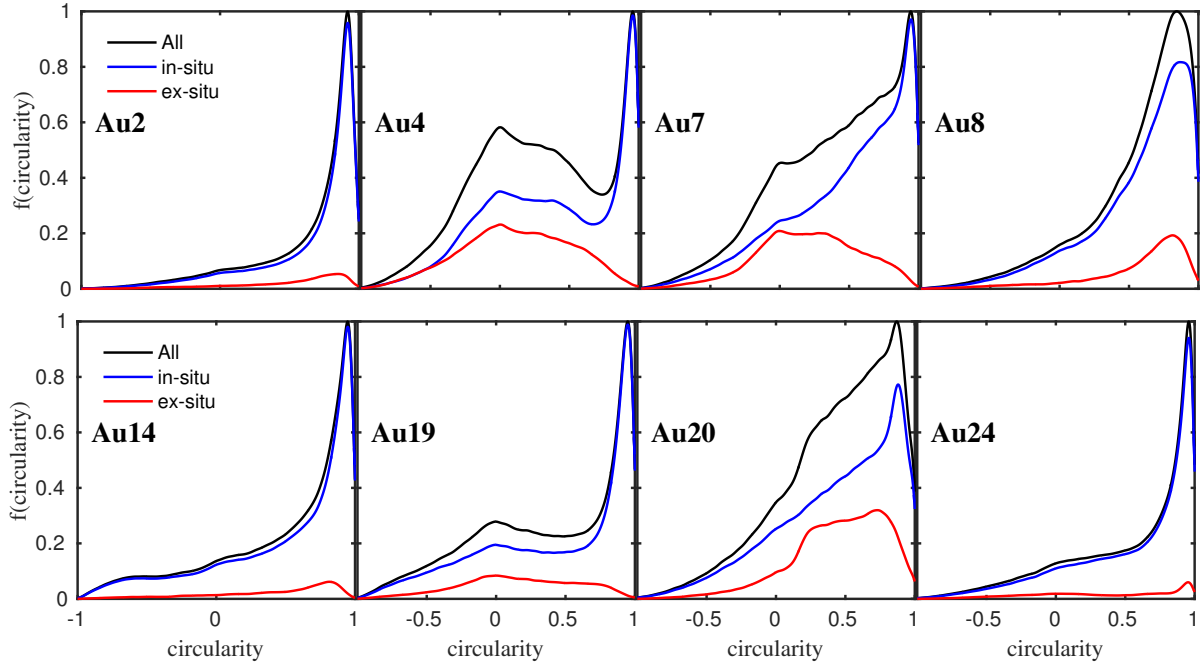


Figure 5. The black lines show the distribution of circularity parameter, ϵ , for all star particles that are located within $R < R_{\text{opt}}$ and $|Z| < 10$ kpc in galaxies with a significant ex-situ disc. The blue and red lines show the contribution from the in-situ and ex-situ stellar populations, respectively.

and this continues until the satellites are fully merged. For example, the Au-2 disc tilts $\sim 60^\circ$ during the merger of the two ex-situ disc most significant contributors. As discussed in Gómez et al. (2016, and references therein), even low-mass satellites that penetrate the outer regions of a galaxy can significantly perturb and tilt a host galactic disc. This is not only due to direct tidal perturbation (e.g. Villalobos & Helmi 2008; Yurin & Springel 2015) but also to the generation of asymmetric features in the DM halo that can be efficiently transmitted to its inner regions, thereby affecting the deeply embedded disc.

Note that the two most significant contributors to the ex-situ disc in Au-2 are accreted onto the host as a group, but they are not bound to each other. This can be seen from their very similar t_{cross} and θ_{infall} values (Table 2). In the remaining galaxies with two significant contributors, the satellites are independently accreted.

6 CHARACTERIZATION OF EX-SITU DISCS

In this Section we characterize the main stellar population properties and the vertical distribution of each ex-situ disc. The left panels of Figure 8 show median $[\text{Fe}/\text{H}]$ profiles as a function of galactocentric distance. The solid lines are the profiles obtained from the ex-situ stellar populations whereas the dashed lines are those obtained from their in-situ counterparts. In all cases, the in-situ $[\text{Fe}/\text{H}]$ profiles show clear negative $[\text{Fe}/\text{H}]$ radial gradients, associated with inside-out formation of the main disc (e.g. Chiappini et al. 2001; Naab & Ostriker 2006; Minchev et al. 2014a, GR17). In general, ex-situ discs also exhibit $[\text{Fe}/\text{H}]$ gradients. These are a reflection of the $[\text{Fe}/\text{H}]$ gradients of the most significant contributors prior to their disruption. Note that the galaxy

Table 2. Main properties of the most significant contributors to the ex-situ discs. The columns are 1) Model name, 2) Satellite's peak total mass, 3) Lookback time at which each satellite crosses the host R_{vir} for the first time, and 4) Angle between the angular momentum vectors of the disc and the satellite orbit, measured at t_{cross} .

Run	$M_{\text{sat}}^{\text{peak}}$ [$10^{11} M_{\odot}$]	t_{cross} [Gyr]	θ_{infall}
Au-2	1.2	8.6	45°
	0.9	8.3	45°
Au-4	5.3	3.1	60°
Au-7	1.8	6	85°
Au-8	1.0	8	25°
Au-14	1.0	7.3	45°
	0.8	9.1	30°
Au-19	2.9	5.8	25°
	0.6	7.1	47°
Au-20	2.5	6	15°
Au-24	0.6	8.6	80°

with the most metal-rich and steepest $[\text{Fe}/\text{H}]$ gradient in the ex-situ disc component is Au-4. As previously discussed, the largest contributor to this ex-situ disc is a $\sim 5.3 \times 10^{11} M_{\odot}$ satellite that crossed the host R_{vir} just ~ 3 Gyr ago.

A detailed analysis of the chemical evolution of the Auriga galaxies will be presented in a forthcoming work. Here we are mainly interested in the differences between the in-situ and ex-situ $[\text{Fe}/\text{H}]$ profiles. We find that, in all cases

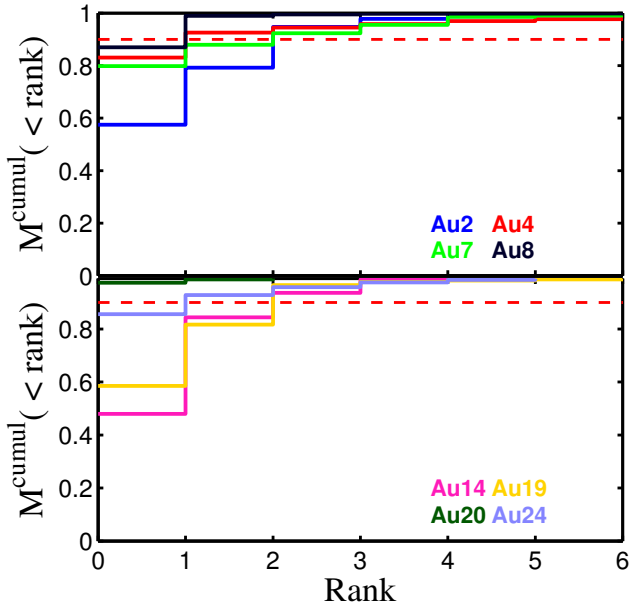


Figure 6. Cumulative stellar mass fractions obtained from each significant ex-situ disc. The step-like cumulative fractions show the contribution from the six most massive contributors to each ex-situ disc in rank order of decreasing mass. The red dashed line shows the 90 per cent level.

and at all radii, ex-situ discs are significantly more metal-poor than their in-situ counterparts. Differences in median metallicity can be as large as ~ 0.5 dex (Au-2, Au-19).

The middle panels of Figure 8 show the median age profiles as a function of galactocentric distance for both stellar populations. In all cases, ex-situ discs (solid lines) show approximately flat age profiles, reflecting the median age of the stellar populations of the most significant satellite contributor. Note that ex-situ discs with younger populations accreted their most significant contributor later on (Au-4, Au-7 and Au-20). Median ages of ex-situ disc populations range between 6 and 9 Gyr. Conversely, the mean age profiles of the in-situ stellar discs show, in general, negative gradients, reflecting their inside-out formation. In addition, this component is significantly younger than the ex-situ disc, with differences in median ages as large as ~ 6 Gyr (e.g. Au-14).

Finally, the right panels of Figure 8 show the ratio of ex-situ to in-situ mass-weighted vertical dispersion, σ_z as a function of galactocentric distance. This quantity provides a measure of disc thickness. In general, we find ex-situ discs to be thicker than the in-situ components, with typical values of $\sigma_z^{\text{ex-situ}}/\sigma_z^{\text{in-situ}} \sim 1.5$. Some galaxies show a clear negative gradient in the outer disc regions ($R \gtrsim 0.5R_{\text{opt}}$, e.g. Au-4, Au-7 and Au-14). As shown by GR17 and Gómez et al. (2017), the in-situ component of these Auriga discs shows strong flaring, warping and bending in the outer regions. This causes $\sigma_z^{\text{in-situ}}$ to rise steeply at galactocentric distances where the disc stops being strongly cohesive due to its weak self-gravity.

The significant differences that the ex-situ and in-situ disc stellar populations exhibit could be used to define in-

dicators to identify ex-situ discs. We discuss this further in Section 7.

7 IDENTIFICATION OF EX-SITU DISCS

In the previous Section we have shown that the median age and $[\text{Fe}/\text{H}]$ of the ex-situ disc stellar populations are older and more metal-poor, respectively, than their in-situ counterparts. Here we explore how these two characteristics could be used to search for this galactic component in our own Galactic disc.

In Figure 9 we show the ex-situ to in-situ mass ratio, ν , obtained from subsets of stellar particles located in different regions of the age and $[\text{Fe}/\text{H}]$ space. As before, we only show four representative examples, but similar results are found for the remaining galaxies with significant ex-situ discs. To generate these two dimensional histograms we first selected all disc stellar particles (recall, $\epsilon \geq 0.7$, $R < R_{\text{opt}}$ and $|Z| < 10$ kpc) located within three different cylindrical shells defined as $(0.2 \pm 0.1, 0.5 \pm 0.1, 0.9 \pm 0.1)R_{\text{opt}}$. On each cylinder we gridded the (Age, $[\text{Fe}/\text{H}]$) space with an $N \times N$ regular mesh of bin size (0.65 Gyr, 0.15 dex). Finally, we computed the ratio ν considering only the stellar particles that are located within each (Age, $[\text{Fe}/\text{H}]$) bin.

The colour bar in Fig. 9 indicates different values of ν . Regions of the (Age- $[\text{Fe}/\text{H}]$) space that are dominated by in-situ stellar populations, i.e. $0 \leq \nu < 1$, are shown in dark blue. It is evident that, at all galactocentric distances, the in-situ disc dominates in regions with young and metal-rich stellar populations. Close to the galactic center, $0.2R_{\text{opt}}$, ex-situ stellar populations are found to dominate at very old ages ($\gtrsim 8$ Gyr) and low $[\text{Fe}/\text{H}]$ ($\lesssim -0.5$ dex). Nonetheless, an interesting pattern arises when larger galactocentric distances are considered. It is clear from this figure that the regions dominated by the ex-situ disc gradually increase as we move further out. In a few examples (Au-14 and Au-24), regions with ages > 6 Gyr are mainly dominated by ex-situ stellar populations already at $0.5R_{\text{opt}}$. Note that, assuming an optical radius of 19 kpc for the Milky Way (Liu et al. 2017), these regions can be regarded as Solar Neighborhood analogs. The trend continues for larger galactocentric distances ($0.9R_{\text{opt}}$). This indicates that the likelihood of identifying an ex-situ disc in samples of old stars increases towards the outskirts of the galactic discs. The reason for this was already discussed in Section 6. In general, the discs in this subset of Auriga galaxies show inside-out formation (see Fig. 8). The in-situ stellar populations become, on average, younger with galactocentric distance. Conversely, we find that the age distribution of the ex-situ population remains nearly constant with galactocentric distance. Thus, as the in-situ populations recede towards regions with younger ages, the ex-situ population takes over.

This can be seen more clearly in Figure 10, where we show Gaussian kernel histograms of the stellar age distribution for the four disc examples previously discussed. Note that no cut in $[\text{Fe}/\text{H}]$ has been imposed to generate these histograms. Again, we can see that close to the galactic center, i.e. $\sim 0.2R_{\text{opt}}$, the in-situ stellar populations (blue lines) dominate these distributions at all ages. As we move outwards, the ex-situ populations (red lines) start to take over at old ages. In all cases, the old tail of these distributions

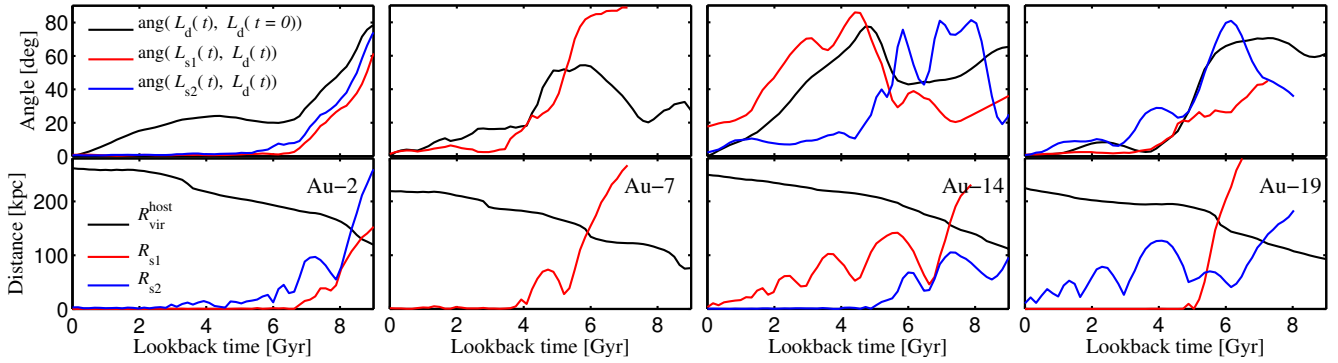


Figure 7. Top panels: The red (blue) lines show the time evolution of the angle between the angular momentum of the disc and that of the orbit of the most significant (second) contributor. The black lines show the time evolution of the orientation of the angular momentum vector of the disc with respect to its orientation at the present-day. Bottom panels: The red (blue) lines show the time evolution of the galactocentric distance of the most significant (second) contributor. The black lines show the time evolution of the host R_{vir} .

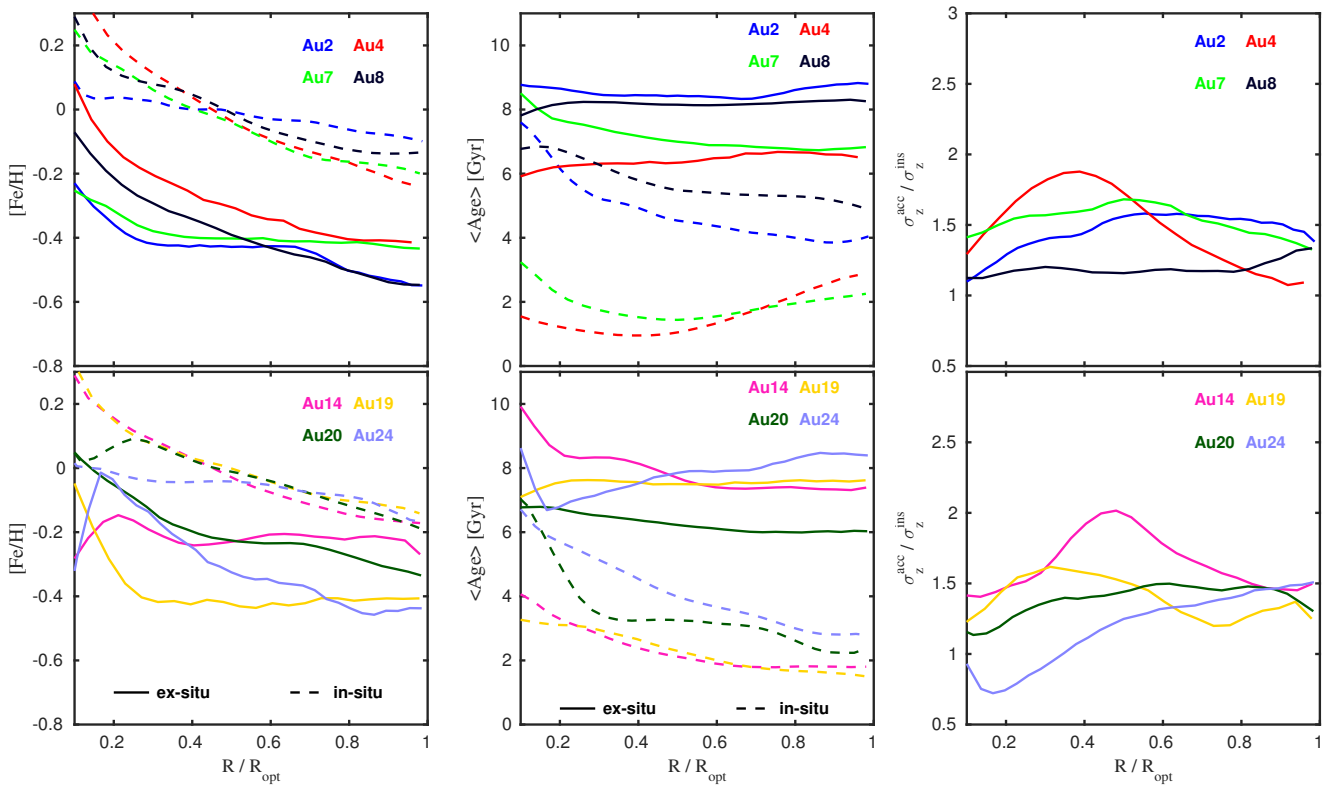


Figure 8. Left and middle panels: Median $[\text{Fe}/\text{H}]$ and age profiles for the discs as a function of galactocentric distance. The solid lines show the profiles obtained from the ex-situ stellar populations whereas the dashed lines give those obtained from their in-situ counterparts. Right panels: ratio of the ex-situ to in-situ mass-weighted vertical dispersions as a function of galactocentric distance.

(age $\gtrsim 7$ Gyr) is dominated by ex-situ star particles at galactocentric distances of $\sim 0.9R_{\text{opt}}$.

It is important to highlight that the presence of an old tail in this distribution does not necessarily imply the presence of an ex-situ disc component. For example, in-situ old stars can be found in the outer regions of a galactic disc as a result of processes such as radial migration (Grand et al. 2016, and references therein). To unambiguously identify ex-situ stars additional information based on chemical tagging should be used (R14, R15).

8 DISCUSSION

In this work we have shown that massive satellites can be disrupted in a plane that is well-aligned with that of the host disc, depositing material on near-circular orbits that are dynamically indistinguishable from those of stars born in-situ. An ex-situ disc would not only be relevant for probing the merger history of the Milky Way, but would also hint at the presence of an underlying DM disc (see e.g. Read et al. 2008; Purcell et al. 2009; Read et al. 2009). The quantification and characterization of the DM discs in the Auriga simulations will be presented in another paper (Schaller et

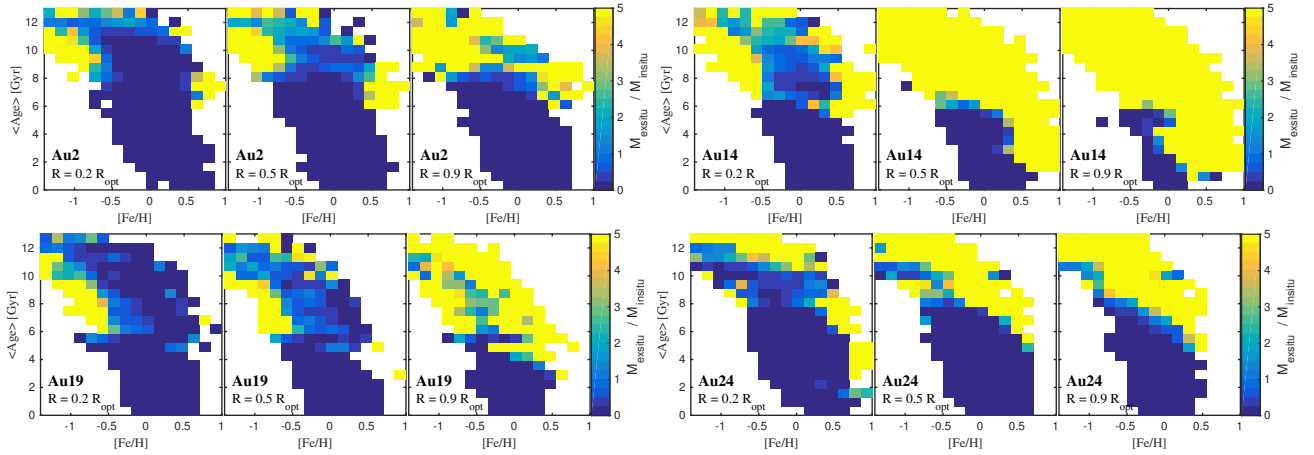


Figure 9. Two dimensional histograms of the ratio of ex-situ to in-situ disc stellar mass, $\nu = M_{\text{exsitu}}/M_{\text{insitu}}$, in age and $[\text{Fe}/\text{H}]$ space, obtained from four representative galaxies with significant ex-situ discs. For each galaxy three panels are shown. Each panel shows the results obtained from the stellar particles located within three different cylindrical shells defined as $(0.2 \pm 0.1, 0.5 \pm 0.1, 0.9 \pm 0.1)R_{\text{opt}}$. Regions dominated by in-situ ($\nu < 1$) and ex-situ ($\nu \geq 5$) disc components are shown in dark blue and yellow, respectively.

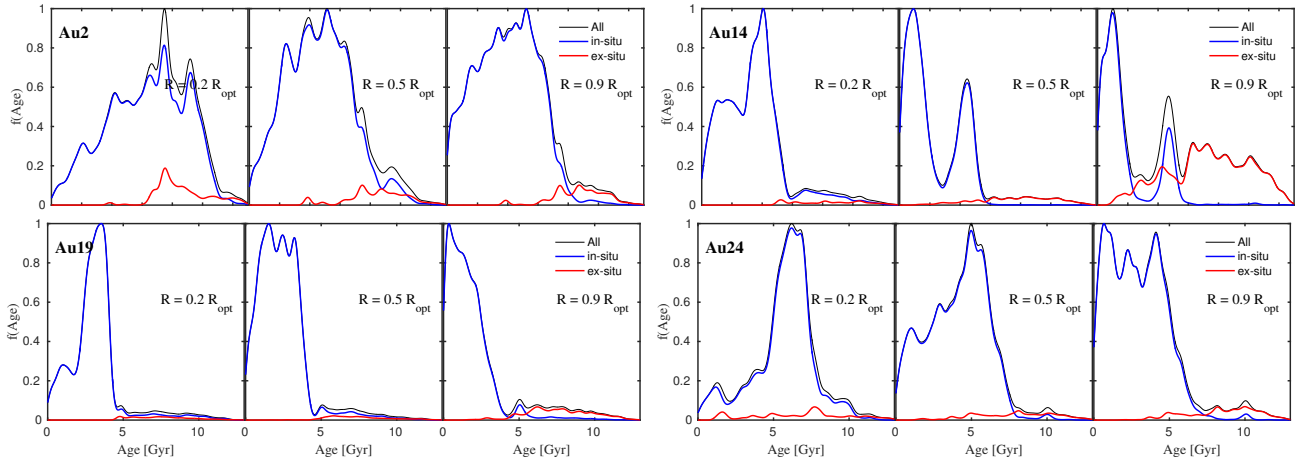


Figure 10. Stellar age distribution of disc particles obtained within the three cylindrical shells used in Figure 9. The red and blue lines show the distributions obtained from the in-situ and ex-situ stellar particles, respectively. The black lines show the overall distributions.

al., in prep). Here we merely show that some of the Auriga galaxies with significant ex-situ discs also have a significant rapidly rotating DM component.

In Figure 11 we show three examples of the velocity distribution of dark matter particles located within a cylinder defined as $|Z| \leq 5$ kpc and $6 \leq R \leq 10$ kpc. In all cases we can see that both the radial, V_{rad} , and the vertical, V_z , velocity components can be well fitted with a single Gaussian centred at 0 km s^{-1} . However, it is clear that a single Gaussian centred at 0 km s^{-1} cannot describe the azimuthal velocity distributions, V_{rot} . Following Read et al. (2009), we used a double Gaussian to describe these distributions. As in Schaller et al. (2016) one of the Gaussian is centred at $V_{\text{rot}} = 0 \text{ km s}^{-1}$. Very similar results are obtained if the center of both Gaussian are left as free parameters. The blue lines show the result of such fits, while the red and green lines show the contribution from each individual Gaussian. In all cases we find the second Gaussian to be centred at high V_{rot} , with values of $\sim 133, 124$ and 126 km s^{-1} for Au-2, Au-8 and Au-20, respectively. Following Schaller et al. (2016),

we estimate the amount of DM that the secondary Gaussian contributes to these cylinders by evaluating its integral. We find contributed mass fractions of 32%, 35% and 50%, respectively. In general, galaxies with significant ex-situ discs show V_{rot} distributions that cannot be described with single Gaussian (Schaller et al. in prep).

The Au-2 case is particularly interesting. It possesses a significant rotating DM component and, as previously discussed, the circularity distribution of its ex-situ component (within the spatially defined disc) peaks at $\epsilon \geq 0.7$ (see also Au-8). The most significant contributors were accreted ~ 8.5 Gyr ago, and quickly merged with the host. More importantly, this galaxy has a smoothly rising age-vertical velocity dispersion relation during the last 8 Gyr of evolution (see Grand et al. 2016, figure 15), and thus its behaviour is qualitatively consistent with that observed in the MW (Casagrande et al. 2011; Minchev et al. 2014b). Recently, Deason et al. (2017, D17) combined Gaia data release 1 astrometry with Sloan Digital Sky Survey (SDSS) images to measure proper motions of old stars in the MW stellar halo.

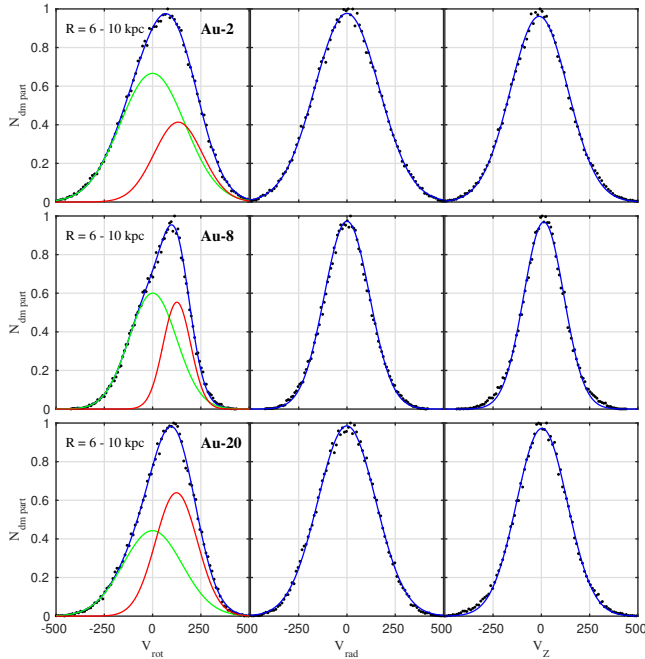


Figure 11. The black dots indicate the velocity distributions of the dark matter particles located within a cylinder defined as $|Z| \leq 5$ kpc and $6 \leq R \leq 10$ kpc. The left, middle and right panels show the rotational, radial and vertical velocity distributions, respectively. The blue lines in the left panels show the result of a double Gaussian fit to the data. The red and green lines show the contributions from each individual Gaussian. The blue lines in the other two panels show the result of single Gaussian fits to the corresponding data.

They find a gently rotating prograde signal, which shows little variation with Galactocentric radius out to 50 kpc. As discussed by D17, some Auriga galaxies with significant ex-situ discs (Au-2, Au-4, Au-7, Au-19 and Au-24) also show mildly rotating old stellar halos, consistent with the observations. An ex-situ component with the characteristics found in e.g. Au-2, and its associated rotating DM component, would not have been detected to date in the MW disc.

9 CONCLUSIONS

We have studied the formation of ex-situ discs in model galaxies with similar mass to the MW, simulated in a fully cosmological context. An important goal of this study was to explore whether a significant ex-situ stellar component could be buried within the near-circular orbit population of the MW disc which is strongly dominated by in-situ stars. For this purpose, we focused our analysis on star particles with large circularity parameter, $\epsilon \geq 0.7$. This differs from the strategy in observational studies, such as those presented by R14 and R15. These attempted to identify an ex-situ disc in the Milky Way by focusing on stars with $0.2 < \epsilon < 0.8$.

Our study shows that approximately one third of our sample (8 out of 26 models) contains a significant ex-situ disc. These galaxies show an ex-situ to in-situ disc ($\epsilon \geq 0.7$) mass ratio $\eta > 0.05$. Note however, that the fraction of models with significant ex-situ discs would be larger if we were

to relax our circularity threshold to lower values. In fact, as shown in Figure 1 of R15, the circularity distributions of the ex-situ stellar discs presented in Read et al. (2008) peak at $\epsilon \sim 0.5$. We find that, in general, the ex-situ to in-situ disc mass fraction rises as we move towards the outer disc regions.

We have characterized the circularity distribution of all stellar particles that are spatially located within regions associated with the galactic discs (i.e. $R < R_{\text{opt}}$ and $|Z| < 10$ kpc). Half of the ex-situ discs sample have a distribution that is consistent with those shown in R15, peaking at values of $\epsilon < 0.7$. Interestingly, for the remaining half we find a circularity distribution that peaks at values of $\epsilon \geq 0.7$. Such discs would not have been detected in existing observational studies.

In general, ex-situ discs are formed from the debris of fewer than three massive satellite galaxies, but most of their mass ($> 50\%$) always comes from a single significant contributor. The peak total mass of this dominant contributor ranges between $6 \times 10^{10} M_{\odot}$ and $5.3 \times 10^{11} M_{\odot}$. Both the virial radius crossing time and the infall angle of these satellites have a very large scatter, with values ranging between 3.1 to 9.1 Gyr and 15° to 85° , respectively. We highlight that significant ex-situ discs can arise from merger events with massive satellites that are accreted at infall angles as large as 85° (see also Read et al. 2009). In these cases we find that the disc and satellite angular momentum vectors rapidly align. This is not purely due to an evolution of the infalling satellite’s orbit, but also to a strong response of the host galactic disc. We find that host discs start to tilt as soon as these massive satellites cross R_{vir} . This tilt can be driven both by direct tidal perturbations (e.g. Villalobos & Helmi 2008; Yurin & Springel 2015; Gómez et al. 2017) and by the generation of asymmetric features in the host DM halo that can extend into the inner regions, affecting the deeply embedded disc (Gómez et al. 2016, and references therein). It is important to note that the response of a disc depends, among other things, on its vertical rigidity. A disc tilts as a whole only in regions where it is strongly cohesive thanks to its self-gravity (e.g. Shen & Sellwood 2006). Thus, the frequency and properties of ex-situ discs may be misrepresented in simulations of Milky Way-like galaxies if these are not able to reproduce correctly the vertical structure of the MW disc (see e.g. Pranav & Jog 2010). This could be an issue for the Auriga simulations, since our final stellar discs are thicker than observed ($h_z \sim 1$ kpc, see GR17). Hence, their vertical rigidity may be significantly lower than that of the MW disc.

Ex-situ discs tend to be thicker than in-situ discs, with vertical dispersion ratios $\sigma_z^{\text{exsitu}}/\sigma_z^{\text{insitu}} \sim 1.5$. In all cases, and at all radii, the ex-situ disc component is significantly more metal-poor than the in-situ disc. Differences in the median [Fe/H] can be as large as 0.5 dex. Ex-situ discs are also significantly older than their in-situ counterparts, with age differences that can be as large as 6 Gyr. Their median age profiles are flat and reflect the median age of the stellar populations from the most significant contributors. In contrast, the median age profiles of the in-situ discs show, in general, negative gradients, reflecting the inside-out formation of these stellar discs.

We have shown that the different properties that the in-situ and ex-situ stellar populations exhibit could be used to

isolate ex-situ star candidates on near-circular orbits in the Milky Way disc (recall, $\epsilon \geq 0.7$). By gridding the Age-[Fe/H] space, and computing the ex-situ to in-situ mass ratio within each bin, we find that the regions dominated by ex-situ disc gradually increase as we move towards the outer disc, while in the inner galactic regions (i.e. $R \sim 0.2R_{\text{opt}}$) in-situ stellar populations dominate nearly everywhere. In a few cases we find that regions with ages > 6 Gyr are dominated by ex-situ disc stars already at galactocentric distances $R = 0.5R_{\text{opt}}$. The likelihood of identifying an ex-situ disc in samples of old stars increases towards the outskirts of the disc. However, the presence of an old tail in the age distribution may not uniquely imply the presence of an ex-situ disc component. To unambiguously identify such an ex-situ component in the MW, additional information based on chemical tagging should be considered.

ACKNOWLEDGEMENTS

We are grateful to Adrian Jenkins and David Campbell for the selection of the sample and making the initial conditions. RG and VS acknowledge support through the DFG Research Centre SFB-881 ‘The Milky Way System’ through project A1. VS and RP acknowledge support by the European Research Council under ERC-StG grant EXAGAL-308037. This work was supported by the Science and Technology Facilities Council (grant number ST/L00075X/1) and the European Research Council (grant number GA 267291, ‘Cosmiway’). This work used the DiRAC Data Centric system at Durham University, operated by the Institute for Computational Cosmology on behalf of the STFC DiRAC HPC Facility (www.dirac.ac.uk). This equipment was funded by BIS National E-infrastructure capital grant ST/K00042X/1, STFC capital grants ST/H008519/1 and ST/K00087X/1, STFC DiRAC Operations grant ST/K003267/1 and Durham University. DiRAC is part of the National E-Infrastructure. SB acknowledges support from the International Max-Planck Research School for Astronomy and Cosmic Physics of Heidelberg (IMPRS-HD) and financial support from the Deutscher Akademischer Austauschdienst (DAAD) through the program Research Grants - Doctoral Programmes in Germany (57129429).

REFERENCES

- Abadi M. G., Navarro J. F., Steinmetz M., Eke V. R., 2003, *ApJ*, **597**, 21
- Antoja T., Valenzuela O., Pichardo B., Moreno E., Figueras F., Fernández D., 2009, *ApJ*, **700**, L78
- Arifanto M. I., Fuchs B., 2006, *A&A*, **449**, 533
- Belokurov V., et al., 2006, *ApJL*, **642**, L137
- Belokurov V., et al., 2007, *ApJ*, **658**, 337
- Binney J., Merrifield M., 1998, *Galactic Astronomy*. Princeton University Press
- Bose S., et al., 2017, *MNRAS*, **464**, 4520
- Casagrande L., Schönrich R., Asplund M., Cassisi S., Ramírez I., Meléndez J., Bensby T., Feltzing S., 2011, *A&A*, **530**, A138
- Chiappini C., Matteucci F., Romano D., 2001, *ApJ*, **554**, 1044
- Cooper A. P., et al., 2010, *MNRAS*, **406**, 744
- Cooper A. P., Parry O. H., Lowing B., Cole S., Frenk C., 2015, *MNRAS*, **454**, 3185
- Cui X.-Q., et al., 2012, *Research in Astronomy and Astrophysics*, **12**, 1197
- Dalton G., 2016, in Skillen I., Barcells M., Trager S., eds, *Astronomical Society of the Pacific Conference Series Vol. 507, Multi-Object Spectroscopy in the Next Decade: Big Questions, Large Surveys, and Wide Fields*. p. 97
- Deason A. J., Belokurov V., Koposov S. E., Gomez F. A., Grand R. J., Marinacci F., Pakmor R., 2017, *ArXiv e-prints*, 1703.09230,
- Gaia Collaboration et al., 2016, *A&A*, **595**, A2
- Gilmore G., et al., 2012, *The Messenger*, **147**, 25
- Gómez F. A., Helmi A., Brown A. G. A., Li Y.-S., 2010, *MNRAS*, **408**, 935
- Gómez F. A., Minchev I., Villalobos Á., O’Shea B. W., Williams M. E. K., 2012, *MNRAS*, **419**, 2163
- Gómez F. A., Minchev I., O’Shea B. W., Beers T. C., Bullock J. S., Purcell C. W., 2013, *MNRAS*, **429**, 159
- Gómez F. A., White S. D. M., Marinacci F., Slater C. T., Grand R. J. J., Springel V., Pakmor R., 2016, *MNRAS*, **456**, 2779
- Gómez F. A., White S. D. M., Grand R. J. J., Marinacci F., Springel V., Pakmor R., 2017, *MNRAS*, **465**, 3446
- Grand R. J. J., Springel V., Gómez F. A., Marinacci F., Pakmor R., Campbell D. J. R., Jenkins A., 2016, *MNRAS*, **459**, 199
- Grand R. J. J., et al., 2017, *MNRAS*,
- Helmi A., de Zeeuw P. T., 2000, *MNRAS*, **319**, 657
- Helmi A., White S. D. M., de Zeeuw P. T., Zhao H., 1999, *Nature*, **402**, 53
- Helmi A., Navarro J. F., Nordström B., Holmberg J., Abadi M. G., Steinmetz M., 2006, *MNRAS*, **365**, 1309
- Helmi A., Williams M., Freeman K. C., Bland-Hawthorn J., De Silva G., 2014, *ApJ*, **791**, 135
- Helmi A., Veljanoski J., Breddels M. A., Tian H., Sales L. V., 2017, *A&A*, **598**, A58
- Ibata R. A., Gilmore G., Irwin M. J., 1994, *Nature*, **370**, 194
- Ibata R., Irwin M., Lewis G. F., Stolte A., 2001, *ApJ*, **547**, L133
- Klement R., Fuchs B., Rix H.-W., 2008, *ApJ*, **685**, 261
- Klement R., et al., 2009, *ApJ*, **698**, 865
- Li R., Frenk C. S., Cole S., Gao L., Bose S., Hellwing W. A., 2016, *MNRAS*, **460**, 363
- Liu C., et al., 2017, *ArXiv e-prints*, 1701.07831,
- Macciò A. V., Ruchayskiy O., Boyarsky A., Muñoz-Cuartas J. C., 2013, *MNRAS*, **428**, 882
- Marinacci F., Pakmor R., Springel V., 2014, *MNRAS*, **437**, 1750
- McCarthy I. G., Font A. S., Crain R. A., Deason A. J., Schaye J., Theuns T., 2012, *MNRAS*, **420**, 2245
- Minchev I., Quillen A. C., Williams M., Freeman K. C., Nordhaus J., Siebert A., Bienaymé O., 2009, *MNRAS*, **396**, L56
- Minchev I., Chiappini C., Martig M., 2014a, *A&A*, **572**, A92
- Minchev I., et al., 2014b, *ApJ*, **781**, L20
- Monachesi A., Gómez F. A., Grand R. J. J., Kauffmann G., Marinacci F., Pakmor R., Springel V., Frenk C. S., 2016, *MNRAS*, **459**, L46
- Monari G., Famaey B., Siebert A., Grand R. J. J., Kawata D., Boily C., 2016, *MNRAS*, **461**, 3835
- Morrison H. L., et al., 2009, *ApJ*, **694**, 130
- Naab T., Ostriker J. P., 2006, *MNRAS*, **366**, 899
- Pakmor R., Springel V., 2013, *MNRAS*, **432**, 176
- Pakmor R., Springel V., Bauer A., Mocz P., Munoz D. J., Ohlmann S. T., Schaaf K., Zhu C., 2016, *MNRAS*, **455**, 1134
- Pakmor R., et al., 2017, *ArXiv e-prints*, 1701.07028,
- Pillepich A., Kuhlen M., Guedes J., Madau P., 2014, *ApJ*, **784**, 161
- Pillepich A., Madau P., Mayer L., 2015, *ApJ*, **799**, 184
- Pranav P., Jog C. J., 2010, *MNRAS*, **406**, 576
- Purcell C. W., Bullock J. S., Kaplinghat M., 2009, *ApJ*, **703**, 2275
- Read J. I., Lake G., Agertz O., Debattista V. P., 2008, *MNRAS*, **389**, 1041

- Read J. I., Mayer L., Brooks A. M., Governato F., Lake G., 2009, [MNRAS](#), **397**, 44
- Ruchti G. R., Read J. I., Feltzing S., Pipino A., Bensby T., 2014, [MNRAS](#), **444**, 515 (R14)
- Ruchti G. R., et al., 2015, [MNRAS](#), **450**, 2874 (R15)
- Sales L. V., et al., 2009, [MNRAS](#), **400**, L61
- Sawala T., et al., 2016, [MNRAS](#), **456**, 85
- Schaller M., Frenk C. S., Fattahi A., Navarro J. F., Oman K. A., Sawala T., 2016, [MNRAS](#), **461**, L56
- Schaye J., et al., 2015, [MNRAS](#), **446**, 521
- Shen J., Sellwood J. A., 2006, [MNRAS](#), **370**, 2
- Springel V., 2010, [MNRAS](#), **401**, 791
- Springel V., et al., 2008, [MNRAS](#), **391**, 1685
- Steinmetz M., et al., 2006, [AJ](#), **132**, 1645
- Villalobos Á., Helmi A., 2008, [MNRAS](#), **391**, 1806
- Vogelsberger M., Zavala J., Loeb A., 2012, [MNRAS](#), **423**, 3740
- Vogelsberger M., Genel S., Sijacki D., Torrey P., Springel V., Hernquist L., 2013, [MNRAS](#), **436**, 3031
- Widrow L. M., Gardner S., Yanny B., Dodelson S., Chen H.-Y., 2012, [ApJ](#), **750**, L41
- Widrow L. M., Barber J., Chequers M. H., Cheng E., 2014, [MNRAS](#), **440**, 1971
- Yurin D., Springel V., 2015, [MNRAS](#), **452**, 2367
- de Jong R. S., et al., 2014, in *Ground-based and Airborne Instrumentation for Astronomy V.* p. 91470M, [doi:10.1117/12.2055826](#)